RSC Advances



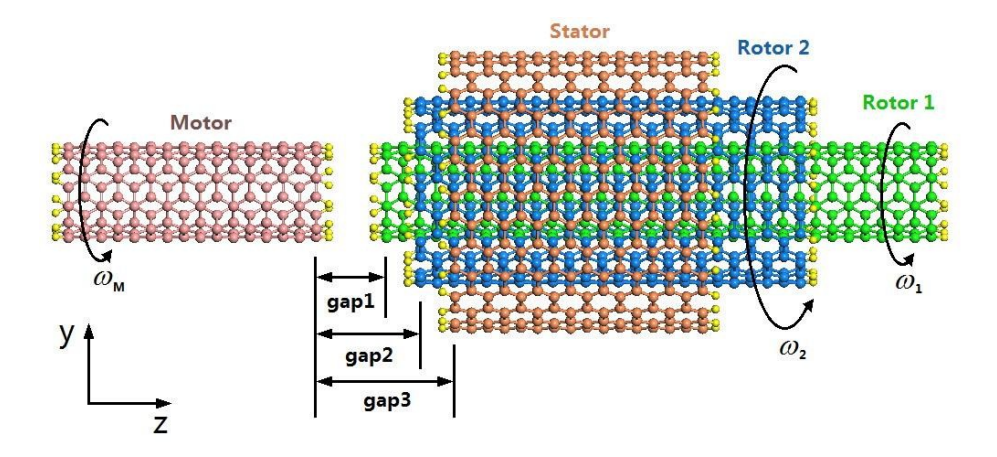
This is an *Accepted Manuscript*, which has been through the Royal Society of Chemistry peer review process and has been accepted for publication.

Accepted Manuscripts are published online shortly after acceptance, before technical editing, formatting and proof reading. Using this free service, authors can make their results available to the community, in citable form, before we publish the edited article. This Accepted Manuscript will be replaced by the edited, formatted and paginated article as soon as this is available.

You can find more information about *Accepted Manuscripts* in the **Information for Authors**.

Please note that technical editing may introduce minor changes to the text and/or graphics, which may alter content. The journal's standard <u>Terms & Conditions</u> and the <u>Ethical guidelines</u> still apply. In no event shall the Royal Society of Chemistry be held responsible for any errors or omissions in this *Accepted Manuscript* or any consequences arising from the use of any information it contains.





A motion transmission system made from coaxial carbon nanotubes is introduced. In the system, the motor is built from a single-walled carbon nanotube and the converter is made from triple-walled carbon nanotubes (TWCNTs). The outer shell acts as a stator with two fixed tube ends. The inner tube (rotor 1) and the middle tube (rotor 2) can move freely in the stator. When the axial gaps between the motor and the TWCNTs are small enough and the motor has a relatively high rotational speed, the two rotors have either stable rotation or oscillation, which can be considered as output signals.

Temperature effects on a motion transmission device made from carbon nanotubes: a molecular dynamics study

Kun Cai ^a, Xiaoni Zhang ^a, Jiao Shi ^a, Qing-Hua Qin ^{b,*}

Abstract

A motion transmission system made from coaxial carbon nanotubes (CNTs) is introduced. In the system, the motor is built from a single-walled carbon nanotube (SWCNT) and the converter is made from triple-walled carbon nanotubes (TWCNTs). The outer shell acts as a stator with two fixed tube ends. The inner tube (rotor 1) and the middle tube (rotor 2) can move freely in the stator. When the axial gaps between the motor and the TWCNTs are small enough and the motor has a relatively high rotational speed, the two rotors have either stable rotation or oscillation, which can be considered as output signals. To investigate the effects of such factors as the length of rotor 2, the rotational speed of the motor, and the environmental temperature on the dynamic response of the two rotors, numerical simulations using molecular dynamics (MD) are presented on a device model having a (5, 5) motor and (5, 5)/(10, 10)/(1, 15) converters. Numerical results show that the two inner tubes can act as both rotor(s) and oscillator, simultaneously if the middle tube is longer than the inner tube. In particular, we find a new phenomenon, mode conversion of the rotation of rotor 1 by changing the environmental temperature. Briefly, rotor 1 rotates synchronously with the high-speed motor at a higher temperature or with rotor 2 at a lower temperature. The effect of radii difference among the three tubes in bearing are also discussed by replace the mid tube (10, 10) with different zigzag tubes.

Keywords: nano-transmission system; carbon nanotube; nano motor; oscillator; molecular dynamics

1. Introduction

CNTs have been shown to have an extraordinary interlayer lubricating feature and other excellent mechanical properties in nanoscale ¹⁻³. Thus, numerous studies over the past decade have focused on fabricating or designing nanodevices from CNTs, such as gigahertz oscillators ^{4,5}, switches ⁶, strain sensors ^{7,8}, bearings ^{9,10}, nanopumps ¹¹⁻¹³, curved nanotube devices ^{14,15}, and motors ¹⁶⁻²². In the internal layers of multi-walled carbon nanotubes (MWCNTs) both rotational and translational motions may exist, features that suggest signal transmission in a nano-device. To investigate interlayer motions in MWCNTs, Fennimore et al. ²³ designed a rotational system using MWCNTs. In that system, a metal plate was glued on the outer tube and driven to rotate by electricity. Investigating the characteristics of the potential barrier of a DWCNT ²⁴, Barreiro et al. ²⁵ observed the relative motion of the outer tube on the long inner tube when a thermal gradient existed along the tube axis. Hamdi et al. ²⁶ proposed a rotary nanomotor made from two axially aligned MWCNTs with opposing chirality. They simulated the motions of the inner tubes when the two segments of system had different charge and found that the motion could vary from pure translational motion to pure rotation according to the combination of chirality of the tubes.

As a nanomotor made from pure carbon nanotubes is difficult to fabricate using the best available techniques ²⁷, MD simulation approaches are usually adopted to present preliminary research into prototypes of such nanodevices.

^a College of Water Resources and Architectural Engineering, Northwest A&F University, Yangling 712100, China

^b Research School of Engineering, the Australian National University, ACT, 2601, Australia

^{*} Corresponding author's email address: qinghua.qin@anu.edu.au

For example, Kang and Hwang ¹⁶ built a fluidic gas driven rotary motor with rotational frequency over 200 GHz according to their simulation results. A gradientless temperature driven motor made from DWCNTs ²¹ can also attain such a high rotational speed. It is expected that temperature-controlled nanodevices would have such advantages as smaller and fewer accessories, easy operation, and good stability, compared to nanodevices driven by either electricity or fluidic gas. Shan et al. ²⁸ studied the electronic transport properties of a silicon nanotube-based field-effect transistor.

In the present study, the temperature effects on the dynamic response of a nanoconverter (Fig. 1) with multiple output signals ²⁹ are studied. In this converter, there is a nanomotor made from a SWCNT with a TWCNT as bearing. The effects of the lengths of the two inner tubes in the bearing, the input speed of the motor, and the temperature on the dynamic behavior of the nanotube system are also considered. The purpose of the present work is to explore a way to design a controllable convertor with multiple output signals.

2. Models and method

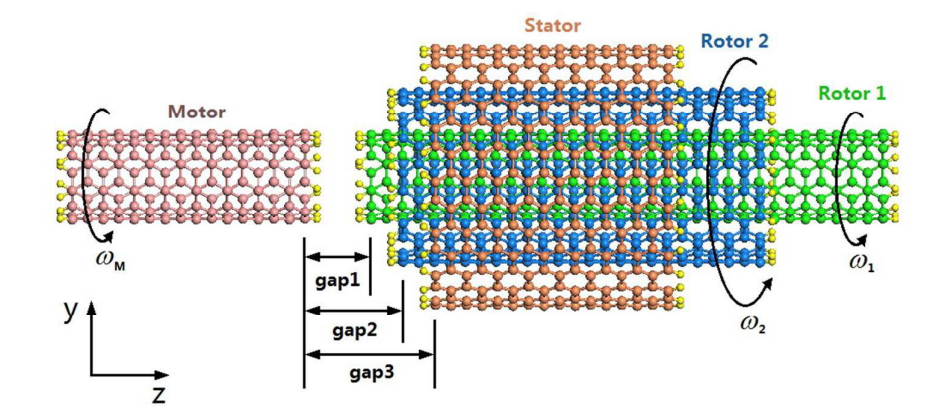


Fig.1 Model of a transmission system made from a (5, 5) SWCNT motor and a (5, 5)/(10, 10)/(15, 15) TWCNT bearing as a converter with **rotor 1** ((5, 5) inner tube), **rotor 2** ((10, 10) middle tube), and **stator** ((15, 15) outer tube), respectively. Each carbon atom at the ends of the tubes is covalently bonded with a hydrogen (small yellow) atom. ω_M , ω_1 , and ω_2 are the rotational frequencies of the motor, rotor 1, and rotor 2, respectively. ω_M is a specified constant as an input signal.

In the system shown in Fig.1, the lengths of the motor, rotor 1, and the stator are fixed. For example, L1, the length of rotor 1, is 4.18 nm, and Ls, the length of the stator, is 1.97 nm. The length of the motor, Lm, is 1.845nm. In the present study, the length of rotor 2, L2, varies between 0.5L1 and 1.5L1, to establish the relationship between the dynamic responses of the two rotors. Here we consider eight cases: L2=2.46, 2.95, 3.44, 3.95 (<L1), 4.42 (>L1), 4.91, 5.41 and 5.93 nm.

The initial values of gap1 and gap2 are 0.335 and 0.588 nm, respectively. The value of gap3 is 0.846 nm and remains unchanged during simulation.

3. Numerical experiments

Before simulation, 100 ps of thermal bath at canonical (NVT) ensemble is applied on the system for relaxation. After relaxation, the dynamic response of the system is simulated within 5 ns at canonical NVT ensemble. The time integral

increment is 1 fs. In simulation, the AIREBO potential ³⁰ is used to instigate the interaction between the carbon and carbon/hydrogen atoms in the system. To determine the effects of environmental temperature on the dynamic response, three different temperatures, 150, 300, and 500 K, are considered. The simulation is carried out using LAMMPS³¹.

3.1 Dynamic response of the two rotors at environmental temperature of $150 \mathrm{K}$ with fixed gap3

(a) When L2<L1

Fig.2 a demonstrates that rotor 1 rotates stably but more slowly than the motor. For example, ~80 GHz of rotor 1 is far lower than the 200 GHz of the motor ($\omega_M = 200$ GHz) (set1 in Table 1). Simultaneously, the rotational speed of rotor 2 is very small, less than 10 GHz.

From Fig.2 b we find that the minimal variation of amplitude in gap1, i.e., the oscillation of the inner tube (rotor 1, blue line), can be neglected. This phenomenon does not depend on either the length of rotor 2 (L2<L1) or the rotational speed of the motor. The oscillation of rotor 2 is not stable when L2=2.95 or 3.44 nm. The oscillation of rotor 2 depends very little on the rotational speed of the motor.

Fig.2 c and Fig.3 c show that rotor 1 rotates synchronously with the motor for any length of rotor 2. Hence, the attraction of the motor to rotor 1 drives their synchronous rotation when ω_M is low, e.g., <100 GHz. Synchronous rotation between the motor and rotor 1 also occurs when ω_M is 50 GHz (Fig.2 e and Fig.3 e). We conclude that synchronous rotation occurs when ω_M is lower than 100 GHz for this system.

(b) When L2>L1

Fig.3 a shows an interesting result, i.e., the two rotors rotating synchronously, with their rotational speed being far lower than that of the motor. ω_1 and ω_2 , the rotational frequencies of the two rotors, are ~35 GHz (set4 in Table 1). Clearly, the attraction of the motor on rotor 1 is not strong enough to induce a high rotational speed of rotor 1. The speed is about 43% of that of rotor 1 as shown in Fig.2 a. The major reason is that the length of rotor 2 is greater than that of rotor 1, i.e., L2>L1. Rotor 2 is excited to rotate at a higher speed due to the higher friction between rotor 1 and rotor 2. Although friction exists between rotor 2 and the stator, the drag of the stator on the rotation of rotor 2 is weaker than the friction between the two rotors. The value of gap2 becomes negative when L2>L1 (Fig.3 b), demonstrating that the interaction between the motor and rotor 2 is also high.

Considering the two rotors as a whole component in the system, we find that the stator and the 200 GHz motor can only drive a \sim 35 GHz coaxial double-rotor component. We therefore conclude that a high-speed (e.g., >200 GHz) rotary motor will drive synchronous rotors in such a system as in Fig.1.

In Fig.3 d, as comparing with the results in Fig.2 d, f, we find that the oscillation of rotor 2 is very stable when L2=4.91 nm and when rotor 2 is driven by the 100 GHz motor, i.e., both the amplitude and the period of the oscillation vary only slightly during the whole simulation except in the period of [2500, 3500] ps. The frequency of oscillation is ~19.5 GHz during [500, 1500] ps. The amplitude is ~0.675 nm. From Fig.3 c (L2=4.91 nm) we find that rotor 1 rotates synchronously with the motor, ω_2 is ~29 GHz, and the rotation is very stable. This observation suggests a way to design rotor 2 with a "rotation+oscillation" mode (Cai et al.⁵). This mode also exists when L2=5.41 nm (Fig.3 c, d). When driven by the 50 GHz motor (Fig.3 f), the mode also exists. This observation implies that it is possible to find a stable oscillator when L2 is within [4.91, 5.41] nm.

Comparing the rotational behavior of rotor 1 shown in Fig.2 e and Fig.3 e, we find that greater fluctuation of the rotational frequency of rotor 1 occurs when the length of rotor 2 is greater than that of rotor 1, i.e., L2>L1.

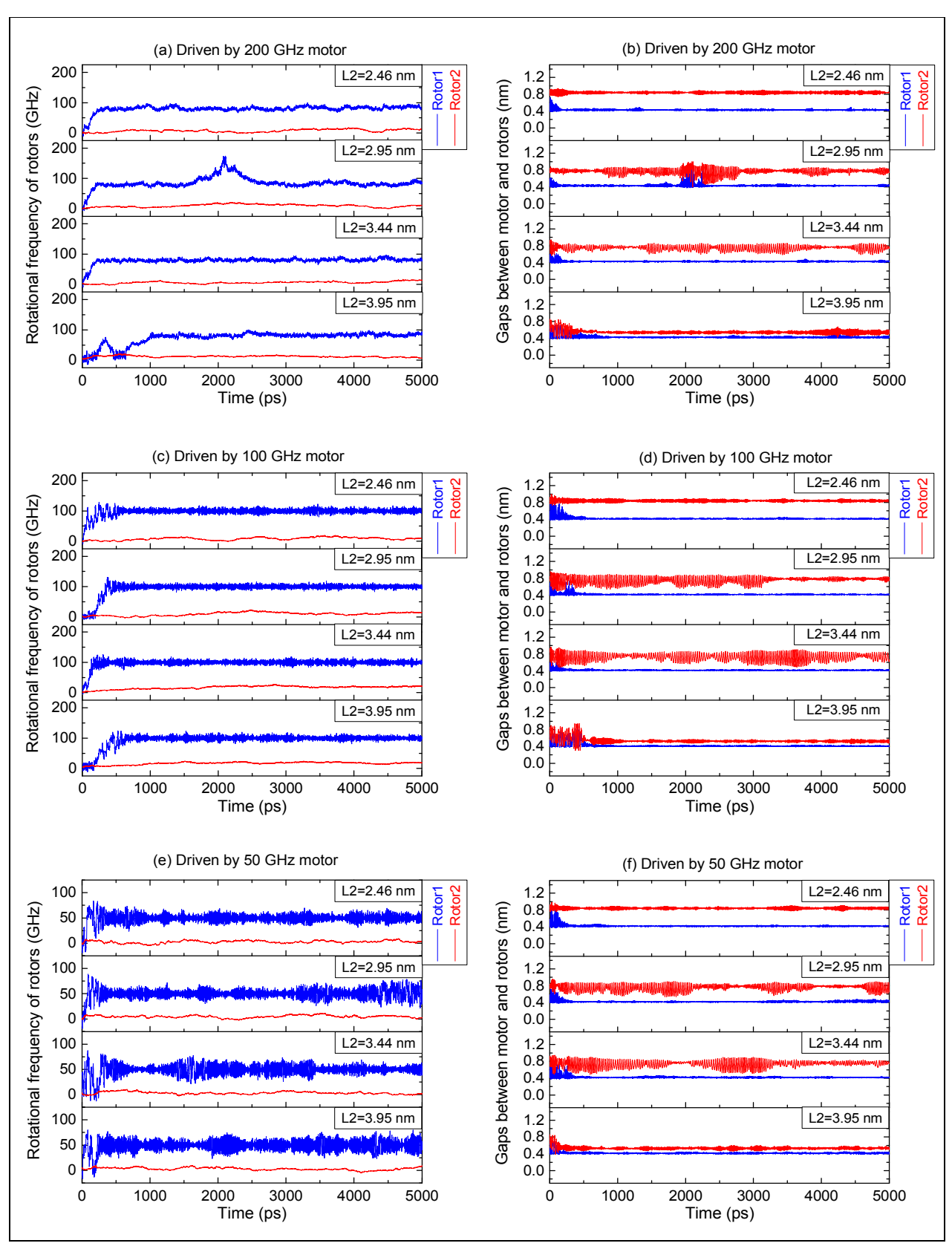


Fig.2 At canonical NVT ensemble with T=150 K, the dynamic response of two rotors (when the length of rotor 2 is less than that of rotor 1, i.e., L2<L1, and driven by the (5, 5) motor at different rotational frequencies).

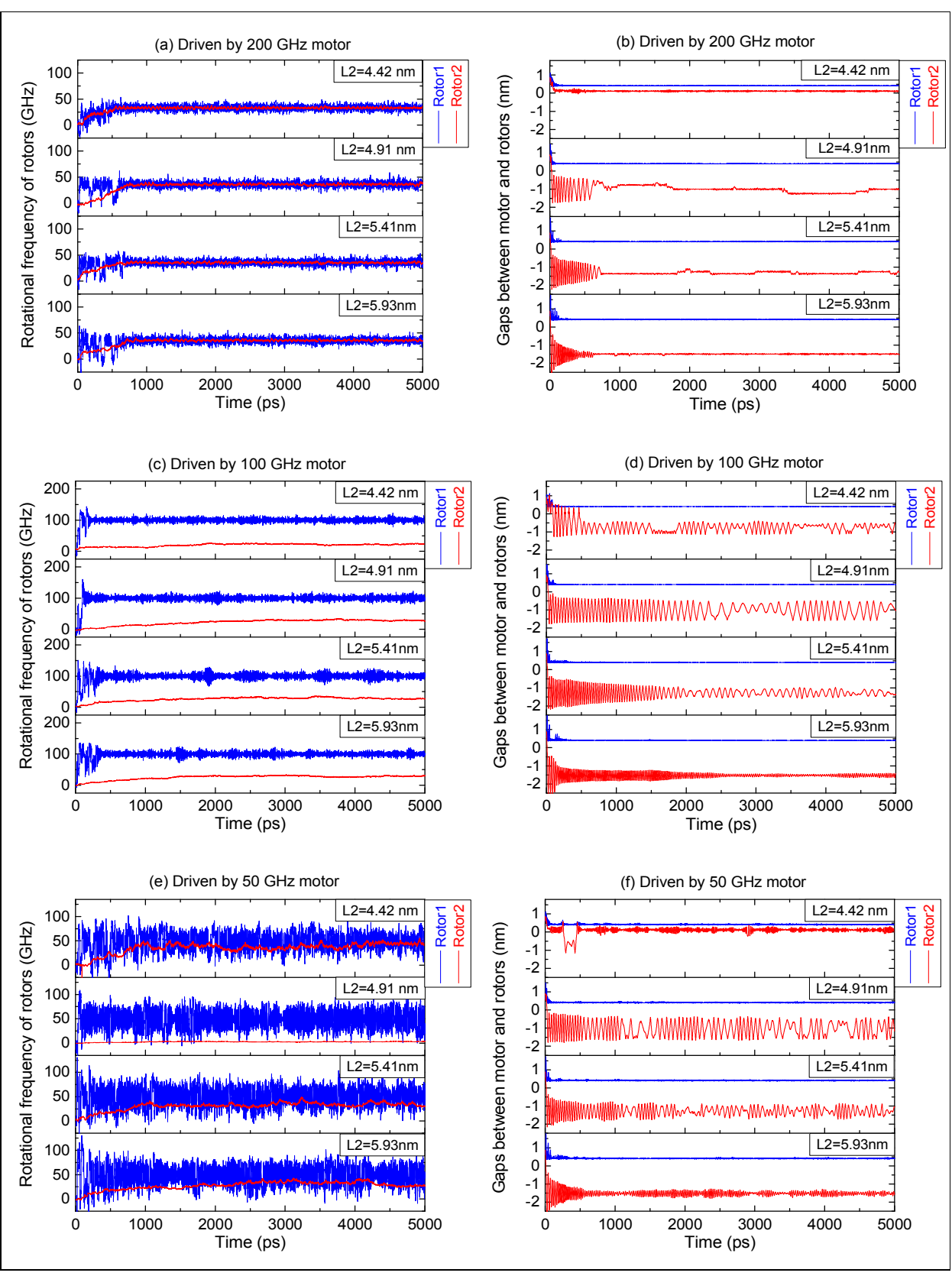


Fig.3 At canonical NVT ensemble with T=150 K, the dynamic response of two rotors when L2>L1, and driven by the (5, 5) motor at different rotational frequencies.

C2/mm Rotor Rotation of rotors C3/millation C	Table 1	Dynamic 1	response of rotors when driven by the (5, 5) motor with different				
Rotor Rot	Set1: Driven by 200 GHz motor and L2 <l1 (fig.2="" a,="" b)<="" td=""></l1>						
Rotor2							
Rotorl In [0, 210] ps, ω, increases to 79.1 GHz and remains stable In [211, 1640] and [2501, 5000] ps, but a peak value of 172.9 In [210, 1640] and [2501, 5000] ps, but a peak value of 172.9 In [211, 1640] and [2501, 5000] ps, but a peak value of 172.9 In [20, 5000] ps, ω₂ is near 9.9 GHz Gaps 2 VVSN 0.762nm, especially in [1900, 2780] ps varying in [0.3961, 1000] nm	2.46			(VVSN) 0.430nm			
Rotor2 In [0,5000] ps, ω₂ is near 9.9 GHz Gap2 VVSN 0.42pmm Gap1 VVSN 0.42pmm Gap1 VVSN 0.42pmm Gap2 VVSN 0.54pmm Gap1 VVSN 0.42pmm Gap1 VVSN 0.42pmm Gap2 VVSN 0.74pmm Gap1 VVSN 0.42pmm Gap2 VVSN 0.74pmm Gap2 VVSN 0.74pmm Gap2 VVSN 0.74pmm Gap2 VVSN 0.74pmm Gap2 VVSN 0.43pmm Gap2 VVSN 0.43pmm		Rotor2		Gap2 VVSN 0.840nm			
$ \begin{array}{c c c c c c c c c c c c c c c c c c c $	2.95	Rotor1	in [211, 1640] and [2501, 5000] ps, but a peak value of 172.9	in [1880, 2290] ps with great fluctuation between 0.376 and			
Stable Rotor2 In [0, 5000] ps, ω2 is near 5.1 GHz Gap2 VVSN 0.742nm				especially in [1900, 2780] ps			
$ \begin{array}{c ccccccccccccccccccccccccccccccccccc$	44	Rotor1		Gap1 VVSN 0.429nm			
$ \begin{array}{c ccccccccccccccccccccccccccccccccccc$			In $[0, 5000]$ ps, ω_2 is near 5.1 GHz	Gap2 VVSN 0.742nm			
Set2: Driven by 100 GHz motor and L2 <l1 (fig.2="" d)="" e,="" l2="" mm<="" td="" =""><td>3.95</td><td></td><td>stable</td><td>Gap1 VVSN 0.431nm</td></l1>	3.95		stable	Gap1 VVSN 0.431nm			
L2/nmRotorRotation of rotorsOscillation of rotors2.46RotorlIn [0, 500] ps, $ω_1$ fluctuates to 99.6GHz and then stays synchronous with motor (SSWM)Gap1 VVSN 0.424nmRotor2In [0, 5000] ps, $ω_2$ is near 8.1 GHzGap2 VVSN 0.840nm2.95Rotor1In [0, 350] ps, $ω_1$ increases to 99.9 GHz and then SSWMGap1 VVSN 0.419nmRotor2 $ω_2$ is between [12.4, 23.1] GHzIn [0, 3200] ps, gap2 varies between [0.954, 0.503] nm; in [3210, 5000] ps, VSN 0.768 nm3.44Rotor1In [0, 165], $ω_1$ increases to 99.9 GHz and then SSWMGap1 VVSN 0.417nmRotor2 $ω_2$ is between [19.7, 27.1] GHzIn [0, 5000] ps, gap2 varies between 0.931 and 0.513 nm3.95Rotor1In [0, 590] ps, $ω_1$ increases to 99.6 GHz and then SSWMGap1 VVSN 0.423nmRotor2 $ω_2$ is between [18.5, 23.7] GHzIn [541, 5000] ps, gap2 VVSN 0.526 nmSet3: Driven by 50 GHz motor and L2 <l1 (fig.2="" e,="" f)<="" td="">L2/nmRotor1$ω_1$ fluctuates but time averagely SSWMGap1 VVSN 0.423nmRotor2In [0, 5000] ps, the average of $ω_2$ is 2.7 GHzGap2 VVSN 0.840nm2.95Rotor1$ω_1$ fluctuates but time averagely SSWMGap1 VVSN 0.422nmRotor2In [0, 5000] ps, the average of $ω_2$ is 3.3 GHzGap2 varies dramatically, but no stable oscillation3.44Rotor1$ω_1$ fluctuates but time averagely SSWMGap1 VVSN 0.424nmRotor2In [0, 5000] ps, the average of $ω_2$ is 3.3 GHzGap2 dramatically varies; in [0, 1780] and [2011, 3910] ps between 0.448 and 0.8573.95Rotor1$ω_1$ fluctuates but</l1>		Rotor2	In [0, 5000] ps, ω_2 is near 12.2 GHz	Gap2 VVSN 0.549nm			
L2/nmRotorRotation of rotorsOscillation of rotors2.46RotorlIn [0, 500] ps, $ω_1$ fluctuates to 99.6GHz and then stays synchronous with motor (SSWM)Gap1 VVSN 0.424nmRotor2In [0, 5000] ps, $ω_2$ is near 8.1 GHzGap2 VVSN 0.840nm2.95Rotor1In [0, 350] ps, $ω_1$ increases to 99.9 GHz and then SSWMGap1 VVSN 0.419nmRotor2 $ω_2$ is between [12.4, 23.1] GHzIn [0, 3200] ps, gap2 varies between [0.954, 0.503] nm; in [3210, 5000] ps, VSN 0.768 nm3.44Rotor1In [0, 165], $ω_1$ increases to 99.9 GHz and then SSWMGap1 VVSN 0.417nmRotor2 $ω_2$ is between [19.7, 27.1] GHzIn [0, 5000] ps, gap2 varies between 0.931 and 0.513 nm3.95Rotor1In [0, 590] ps, $ω_1$ increases to 99.6 GHz and then SSWMGap1 VVSN 0.423nmRotor2 $ω_2$ is between [18.5, 23.7] GHzIn [541, 5000] ps, gap2 VVSN 0.526 nmSet3: Driven by 50 GHz motor and L2 <l1 (fig.2="" e,="" f)<="" td="">L2/nmRotor1$ω_1$ fluctuates but time averagely SSWMGap1 VVSN 0.423nmRotor2In [0, 5000] ps, the average of $ω_2$ is 2.7 GHzGap2 VVSN 0.840nm2.95Rotor1$ω_1$ fluctuates but time averagely SSWMGap1 VVSN 0.422nmRotor2In [0, 5000] ps, the average of $ω_2$ is 3.3 GHzGap2 varies dramatically, but no stable oscillation3.44Rotor1$ω_1$ fluctuates but time averagely SSWMGap1 VVSN 0.424nmRotor2In [0, 5000] ps, the average of $ω_2$ is 3.3 GHzGap2 dramatically varies; in [0, 1780] and [2011, 3910] ps between 0.448 and 0.8573.95Rotor1$ω_1$ fluctuates but</l1>	Set2: Driven by 100 GHz motor and L2 <l1 (fig="" 2="" c="" d)<="" td=""></l1>						
	L2/nm	Rotor	, <u> </u>				
$ \begin{array}{c ccccccccccccccccccccccccccccccccccc$		Rotor1		Gap1 VVSN 0.424nm			
$ \begin{array}{c ccccccccccccccccccccccccccccccccccc$		Rotor2		Gap2 VVSN 0.840nm			
$ \begin{array}{c ccccccccccccccccccccccccccccccccccc$	2.95	Rotor1		-			
$ \begin{array}{c ccccccccccccccccccccccccccccccccccc$		Rotor2		between [0.954, 0.503] nm; in			
$ \begin{array}{c ccccccccccccccccccccccccccccccccccc$	3.44	Rotor1					
$ \begin{array}{c ccccccccccccccccccccccccccccccccccc$			ω_2 is between [19.7, 27.1] GHz	between 0.931 and 0.513 nm			
	3.95	Rotor1					
		Rotor2	ω_2 is between [18.5, 23.7] GHz				
$ \begin{array}{c ccccccccccccccccccccccccccccccccccc$	Set3: Driven by 50 GHz motor and L2 <l1 (fig.2="" e.="" f)<="" td=""></l1>						
$ \begin{array}{c ccccccccccccccccccccccccccccccccccc$	L2/nm	Rotor	Rotation of rotors	Oscillation of rotors			
$ \begin{array}{c ccccccccccccccccccccccccccccccccccc$	2.46			-			
Rotor2 In [0, 5000] ps, the average of ω_2 is 3.3 GHz Gap2 varies dramatically, but no stable oscillation 3.44 Rotor1 ω_1 fluctuates but time averagely SSWM Gap1 VVSN 0.424nm Rotor2 In [0, 5000] ps, the average of ω_2 is 3.3 GHz Gap2 dramatically varies; in [0, 1780] and [2011, 3910] ps between 0.448 and 0.857 3.95 Rotor1 ω_1 fluctuates but time averagely SSWM Gap1 VVSN 0.419nm Rotor2 In [0, 5000] ps, the average of ω_2 is 1.5 GHz Gap2 VVSN 0.534nm Set4: Driven by 200 GHz motor and L2>L1 (Fig.3 a, b) L2/nm Rotor Rotation of rotors Oscillation of rotors 4.42 Rotor1 In [0, 490] ps, ω_1 increases to 33.0 GHz and then remains Gap1 VVSN 0.418nm				-			
$ \begin{array}{c ccccccccccccccccccccccccccccccccccc$	2.95			1			
Rotor2 In [0, 5000] ps, the average of ω_2 is 3.3 GHz Gap2 dramatically varies; in [0, 1780] and [2011, 3910] ps between 0.448 and 0.857 3.95 Rotor1 ω_1 fluctuates but time averagely SSWM Gap1 VVSN 0.419nm Rotor2 In [0, 5000] ps, the average of ω_2 is 1.5 GHz Gap2 VVSN 0.534nm Set4: Driven by 200 GHz motor and L2>L1 (Fig.3 a, b) L2/nm Rotor Rotation of rotors Oscillation of rotors 4.42 Rotor1 In [0, 490] ps, ω_1 increases to 33.0 GHz and then remains Gap1 VVSN 0.418nm		Rotor2	In [0, 5000] ps, the average of ω_2 is 3.3 GHz	stable oscillation			
	3.44						
Rotor2 In [0, 5000] ps, the average of ω_2 is 1.5 GHz Gap2 VVSN 0.534nm Set4: Driven by 200 GHz motor and L2>L1 (Fig.3 a, b) L2/nm Rotor Rotation of rotors Oscillation of rotors 4.42 Rotor1 In [0, 490] ps, ω_1 increases to 33.0 GHz and then remains Gap1 VVSN 0.418nm		Rotor2	In [0, 5000] ps, the average of ω_2 is 3.3 GHz	1780] and [2011, 3910] ps			
Set4: Driven by 200 GHz motor and L2>L1 (Fig.3 a, b) L2/nm Rotor Rotation of rotors Oscillation of rotors 4.42 Rotorl In [0, 490] ps, $ω_1$ increases to 33.0 GHz and then remains Gap1 VVSN 0.418nm	3.95	Rotor1	ω_1 fluctuates but time averagely SSWM	Gap1 VVSN 0.419nm			
L2/nmRotorRotation of rotorsOscillation of rotors4.42Rotor1In $[0, 490]$ ps, $ω_1$ increases to 33.0 GHz and then remainsGap1 VVSN 0.418nm		Rotor2	In $[0, 5000]$ ps, the average of ω_2 is 1.5 GHz	Gap2 VVSN 0.534nm			
4.42 Rotor1 In [0, 490] ps, ω_1 increases to 33.0 GHz and then remains Gap1 VVSN 0.418nm							
	4.42	Rotor1		Gap1 VVSN 0.418nm			

	Rotor2	Stays synchronous with rotor 1	Gap2 VVSN 0.118nm	
4.91	Rotor1	In [0, 590] ps, ω_1 increases to 35.8 GHz and then remains stable	Gap1 VVSN 0.413nm	
	Rotor2	Stays synchronous with rotor 1	In [0, 780] ps, varies between [-1.746, 0.017] nm, and VVSN -1.012 nm later	
5.41	Rotor1	In [0, 410] ps, ω_1 increases to 35.4 GHz and then remains stable	Gap1 VVSN 0.414nm	
	Rotor2	Stays synchronous with rotor 1	In [0, 740] ps, varies between -2.224 and 0.069 nm	
5.93	Rotor1	In [0, 550] ps, ω_1 increases to 35.5 GHz and then remains stable	Gap1 VVSN 0.417nm	
	Rotor2	Stays synchronous with rotor 1	In [0, 620] ps, varies in [-2.624, 0.084] nm, and VVSN -1.495 nm later	
Set5: Driven by 100 GHz motor and L2>L1 (Fig.3 c, d)				
I 2/nm	Dotor	Potation of rators	Oscillation of rotors	

L2/nm	Rotor	Rotation of rotors	Oscillation of rotors
4.42	Rotor1	In $[0, 65]$ ps, ω_1 increases to 100.2GHz and SSWM	Gap1 VVSN 0.405nm
	Rotor2	In $[0, 2100]$, ω_2 increases to 22.6GHz and then remains	In [0, 450] ps, varies in [-1.256,
		stable	0.879] nm, and varies near
			-0.768 nm later
4.91	Rotor1	In $[0, 100]$ ps, ω_1 fluctuates to 100.2 GHz and SSWM	Gap1 VVSN 0.405nm
	Rotor2	In [0, 2750] ps, ω_2 increases to 29.4 GHz and then remains	In [0, 2200] ps, varies
		stable	harmoniously in [-1.740, 0.893]
			nm
5.41	Rotor1	In [0, 410] ps, ω_1 fluctuates to 100.1 GHz and SSWM	Gap1 VVSN 0.407nm
	Rotor2	In [0, 2650] ps, ω_2 increases to 29.4 GHz and then remains	Shows slow damping in [-2.120,
		stable	-0.076] nm
5.93	Rotor1	In [0, 410] ps, ω_1 fluctuates to 100.0 GHz and SSWM	Gap1 VVSN 0.409nm
	Rotor2	In [0, 2020] ps, ω_2 increases to 29.0GHz and then remains	In [200, 1600] ps, varies
		stable	harmoniously in [-1.964, -1.081]
			nm

Set6: Driven by 50 GHz motor and L2>L1 (Fig. 3 e, f)					
L2/nm	Rotor	Rotation of rotors	Oscillation of rotors		
4.42	Rotor1	ω_1 fluctuates but time averagely SSWM	Gap1 VVSN 0.405nm		
	Rotor2	In [0, 1000] ps, ω_2 increase to 39.2 GHz and then remains	Beyond [450, 5000] ps, gap2		
		stable	VVSN 0.117 nm		
4.91	Rotor1	ω_1 fluctuates but time averagely SSWM	Gap1 VVSN 0.405nm		
	Rotor2	Almost no rotation in [0, 5000] ps	In [0, 1100] and [1600, 3000]		
			ps, harmoniously varies in		
			[-1.679, -0.359] nm		
5.41	Rotor1	ω_1 fluctuates but time averagely SSWM	Gap1 VVSN 0.407nm		
	Rotor2	In $[0, 1050]$ ω_2 increases to 33.8 GHz and then remains	Shows damping in [0, 5000] ps		
		stable			
5.93	Rotor1	ω_1 fluctuates but time averagely SSWM	Gap1 VVSN 0.409nm		
	Rotor2	In [0, 3140] ps, ω_2 increases to 39.2 GHz and then remains	Shows quick damping in [0,		
		stable	600] ps, and varies nearby		
			-1.527 nm latter		

3.2 Dynamic response of the two rotors at 300K

At 300 K (higher than the 150 K mentioned above), the rotation and oscillation of the two rotors are shown in Fig.4 and Fig.5 when they are driven by the (5, 5) motor with different speeds. Comparison of the results in Fig.2 and Fig.3 at 150 K demonstrates some peculiar characteristics.

(a) When L2 < L1

First, ω_1 and ω_2 vary between [82, 85] GHz and [10, 20] GHz respectively, when driven by the 200 GHz motor. The oscillation of the two rotors is poor, as is the case for the two rotors at 150 K.

Second, rotor 1 rotates synchronously with the motor as long as the rotational frequency of the motor is no higher than 100 GHz. Gap1 varies slightly near 0.43 nm and gap2 varies obviously for [0, 5000] ps.

Third, ω_2 is very stable when L2=3.95 nm (very close to L1), e.g., ~22 GHz driven by the 200 GHz motor, ~26 GHz by the 100 GHz motor and ~27 GHz by the 50 GHz motor, when the difference between L1 and L2 is very small. This finding implies that ω_2 depends slightly on the rotational speed of the motor. It is significant knowledge for designing a rotor with stable rotational speed in a NEMS.

(b) When L2>L1

Fourth, the two rotors rotate synchronously only when ω_M is 200 GHz and L2=4.42 nm. If L2>4.42nm, rotor 1 rotates synchronously with the motor rather than with rotor 2. At the same time, rotor 2 rotates stably with ~60 GHz of rotational frequency, which is independent of L2(>4.42 nm).

Fifth, when ω_M is no higher than 100 GHz, rotor 1 rotates synchronously with the motor and rotor 2 rotates very stably and the rotational speed is ~38 GHz. In particular, ω_2 is independent of L2(>L1), which is significant for designing a stable nanorotor.

Sixth, the oscillation of rotor 2 performs better when driven by the 100 GHz motor with L2=4.91 nm or when driven by the 50 GHz motor with L2=5.41 nm.

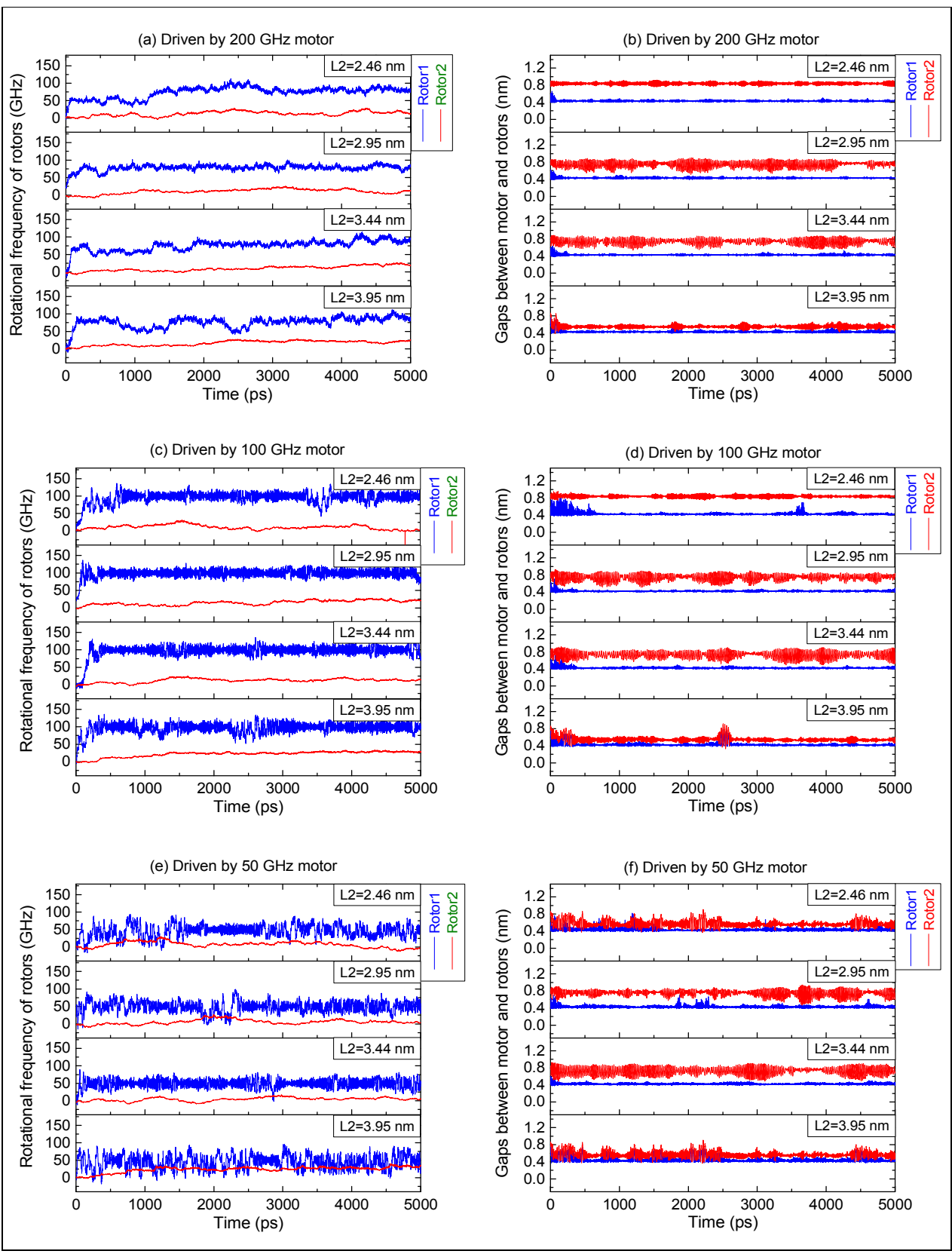


Fig.4 At canonical NVT ensemble with T=300 K, the dynamic response of two rotors when L2<L1, and driven by the (5, 5) motor at different rotational frequencies.

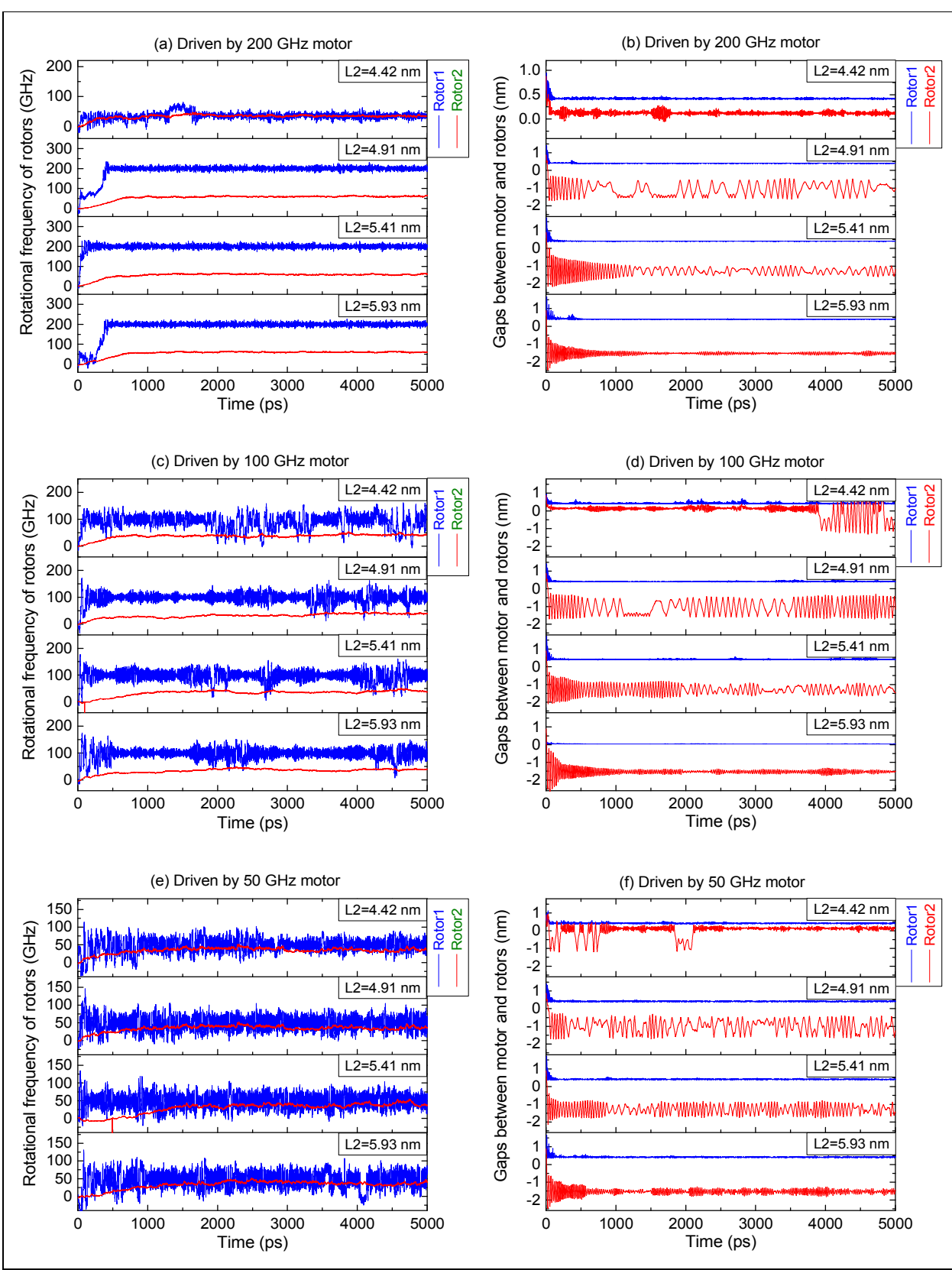


Fig.5 At canonical NVT ensemble with T=300 K, the dynamic response of two rotors when L2>L1, and driven by the (5, 5) motor at different rotational frequencies.

3.3 Dynamic response of the two rotors at 500K

(a) When L2<L1

When driven by the 200 GHz motor (Fig.6 a, b), the rotation of the rotor 1 is unstable and rotor 2 has almost no rotation or oscillation. Particularly when L2=3.44nm, the two rotors have no speed of either rotation or oscillation. Gap1 varies from 0.443 nm to 0.425 nm and gap 2 varies from 0.835 nm to 0.596 nm as L2 changes from 2.46 nm to 3.95 nm. This effect occurs because the attraction of the motor to rotor 1 is strong and the right end of rotor 2 is between the right ends of rotor 1 and the stator. Hence, the gaps decrease with the increase of L2.

When driven by the 100 GHz motor (Fig.6 c, d), rotor 1 maintains synchronous rotation with the motor after a period of acceleration. Rotor 2 has a very low rotational frequency. When L2=3.44 nm, the two rotors have no rotation. The oscillation of the two rotors is similar to that when they are driven by the 200 GHz motor (Fig.6 f).

When driven by the 50 GHz motor (Fig.6 e, f), rotor 1 generally rotates synchronously with the motor. When L2=3.44 nm, the two rotors have no oscillation or rotation.

From the above, we find that the dynamic response of the two rotors is peculiar when L2=3.44 nm. For instance, the rotors may have no rotation when the rotational speed of the motor is greater than 100 GHz or have no oscillation when the motor has a low rotational speed.

(b) When L2>L1

When driven by the 200 GHz motor (Fig.7 a, b), the dynamic response of the two rotors is very similar to that at 300 K. For instance, the two rotors rotate synchronously with a rotational speed of ~47GHz when L2=4.42 nm. If L2>4.42 nm, rotor 1 rotates synchronously with the motor, and the rotational frequency of rotor 2 is ~67 GHz and ω_2 varies very slightly during [1000, 5000] ps.

When driven by the 100 GHz motor (Fig.7 c, d), rotor 1 has no oscillation and the rotational frequency is time averagely identical to that of the motor. Rotor 2 has both perfect oscillation and very stable rotation when L2=4.91 nm.

When driven by the 50 GHz motor, the two rotors rotate almost synchronously when L2=4.42 nm. When L2>4.42 nm, the rotation of rotor 2 is stable. Notably, the oscillation of rotor 2 is also perfect when L2 varies within [4.91, 5.41] nm.

From the data in Figures (2-7), we conclude that the oscillation of the rotors is very poor when L2<L1 at any environmental temperature and driven by the motor with any rotational frequency. When L2>L1, the value of gap2 becomes negative, which means that the joint between the motor and rotor 1 enters into the shell of rotor 2, resulting in a better dynamic response of rotor 2.

In particular, rotor 2 has very stable rotational speed and oscillation when L2=4.91 nm or 5.41 nm. The major reason is that the right end of rotor 2 is locked between the right ends of the stator and rotor 1 which has no oscillation, and the interaction between the left ends of rotor 2 and the stator is strong. Therefore, we suggest a potential design of a device that has simultaneous stable oscillation and rotation from such a system with L2>L1.

If L2=5.93, we can obtain a pure double-rotor system with no oscillation when driven by a 200GHz motor at any temperature. This effect occurs mainly because the total length of the motor connecting with rotor 1 is nearly equal to L2. Hence, rotor 2 has no obvious amplitude when oscillating. On the other hand, we can also design a device in which rotor 2 acts as a pure rotator when the right (or left) end of rotor 2 is fixed within a small gap between the corresponding ends of the motor and the stator.

When L2 is no less than 4.91 nm and the rotors are driven by a high-speed (e.g., 200 GHz) motor, the resultant effect suggests a way to convert the rotational modes of the two rotors by changing the environmental temperature. For instance, rotor 1 rotates synchronously with the motor at a lower temperature (e.g., 150 K in Fig.3 a) or with rotor 2 at

a higher temperature (300K in Fig.5 or 500 K in Fig.7). The reason is that the thermal vibration of atoms on tubes increases the interaction among them, and the interaction between the motor and rotor 1 is stronger than that between the two rotors.

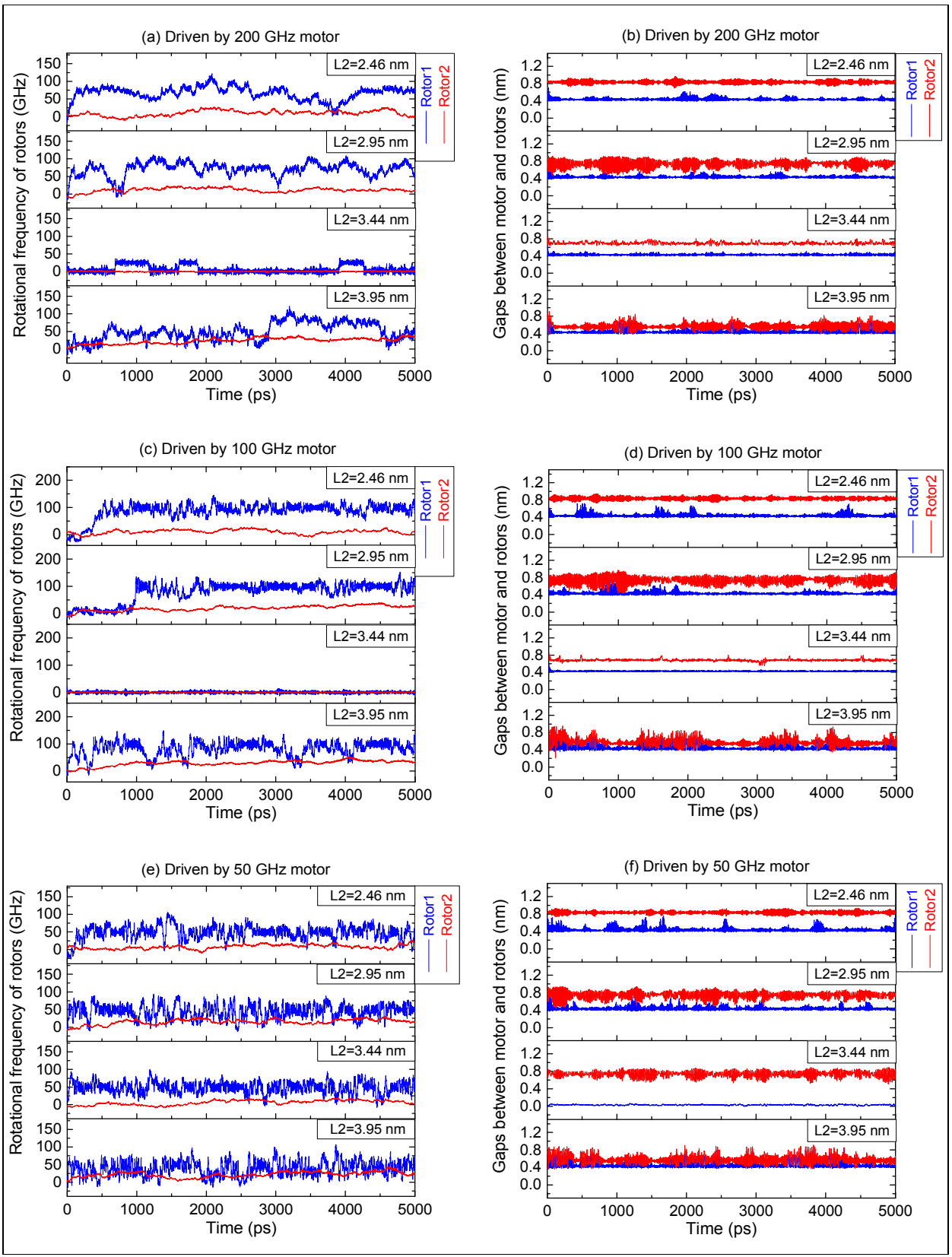


Fig.6 At canonical NVT ensemble with T=500 K, the dynamic response of two rotors when L2<L1, and driven by the (5, 5) motor at different rotational frequencies.

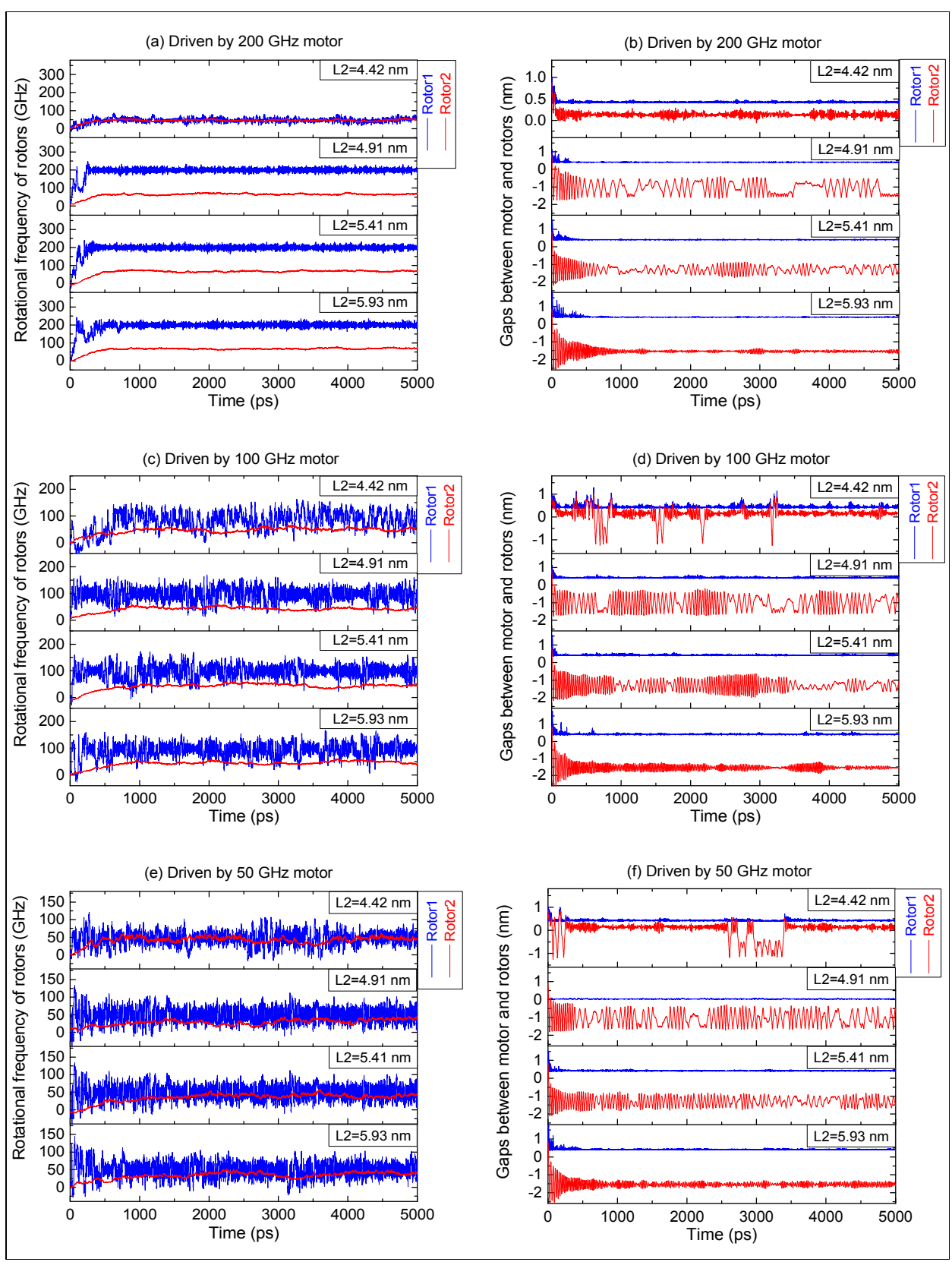


Fig.7 At canonical NVT ensemble with T=500 K, the dynamic response of two rotors when L2>L1, and driven by the (5, 5) motor at different rotational frequencies.

3.4 Effects of radii difference between the two rotors

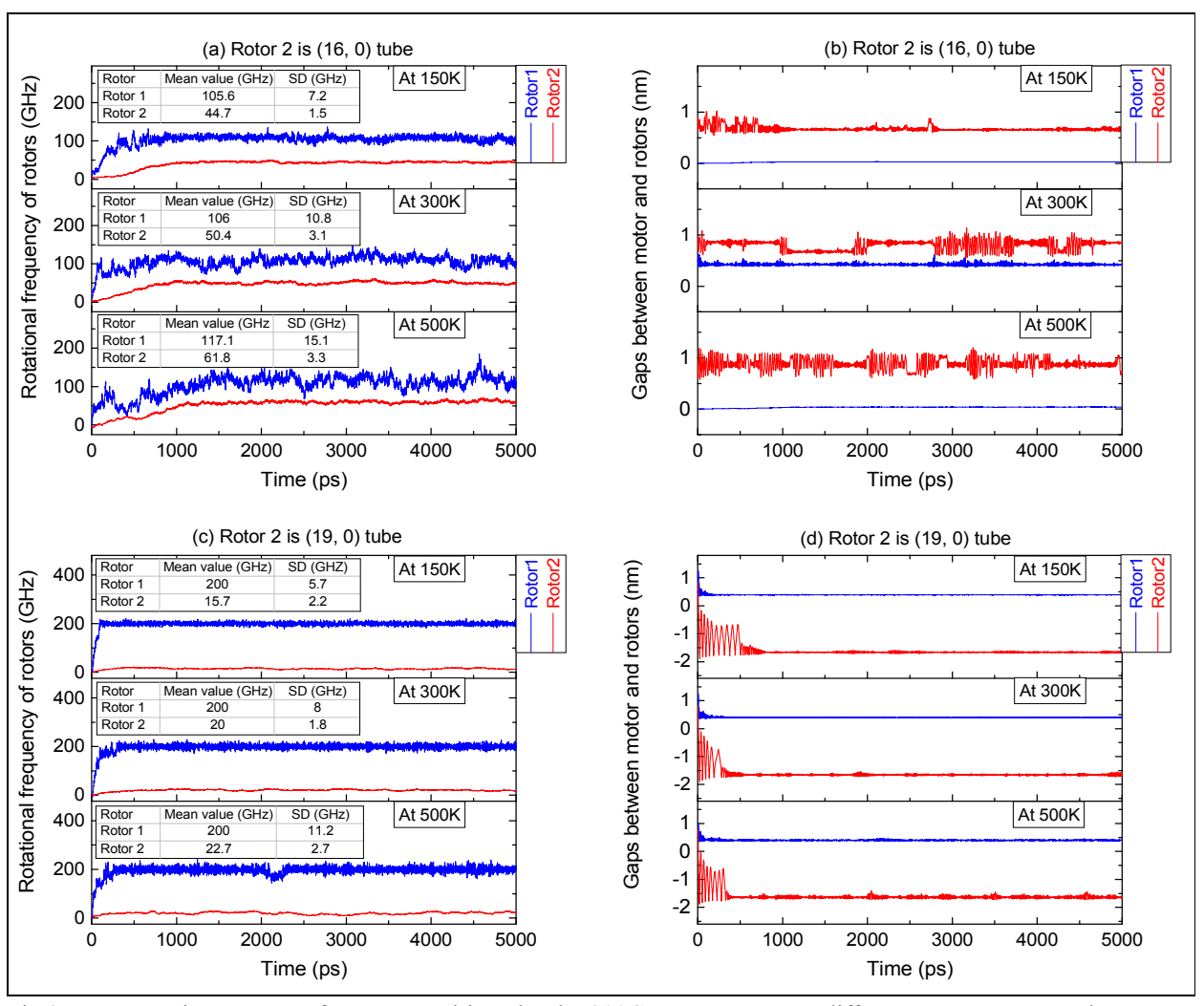


Fig.8 Dynamic response of two rotors driven by the 200GHz motor and at different temperature. In the system, the length of zigzag rotor 2 is 5.112 nm. The mean value and standard deviation (SD) are counted during [4001, 5000] ps.

To investigate the effect of radii difference between two rotors on the dynamic response of the system, the original (10, 10) rotor 2 is replaced with zigzag tube, e.g., (16, 0) with diameter of 1.253 nm<1.356 nm of (10, 10) tube or (19, 0) with diameter of 1.487 nm>1.356nm. Hence, the radii difference between (16, 0) rotor 2 and (5, 5) rotor 1 is smaller than 0.334 nm, and the radii difference between (19, 0) rotor 2 and (5, 5) rotor 1 is greater than 0.334 nm.

Due to the smaller inter tube distance between (16, 0) rotor 2 and rotor 1, the friction between two tubes is greater than that between (10, 10) rotor 2 and rotor 1. Therefore, the rotational frequency of rotor 1 is far less than motor's speed, i.e., 200 GHz. And the rotational frequency of (16, 0) rotor 2 is no less than that of (10, 10) rotor 2. The oscillation of the rotor 1 can be neglected. The oscillation of (16, 0) rotor 2 is not stable at higher temperature, e.g., 300 K or 500 K. And the value of gap2 is always positive due to the smaller radii difference between (16, 0) and (5, 5) tubes.

For the similar reason of friction between two rotors, the rotor 1 rotates synchronously with the motor and the (19,

0) rotor 2 has very small rotational frequency than the (10, 10) rotor 2. The oscillation of either rotor 1 or rotor 2 can be neglected. The value of gap2 is negative because of the higher radii difference between (19, 0) and (5, 5) than that between (10, 10) and (5, 5) tubes.

From the statistical results, one can also find that the two rotors rotate with higher speed at higher temperature. The major reason is that the interaction between two rotors increases with an increase in the temperature.

4. Conclusions

From the simulation results for the dynamic responses of the rotors in a complex transmission system, some remarkable conclusions are drawn for the design of a controllable convertor.

- (1) The oscillation of the rotors is very poor when L2 <L1 at any environmental temperature and when they are driven by a motor with any rotational frequency.
- (2) When L2>L1, rotor 2 has a very stable rotational speed and oscillation when L2=4.91 nm or 5.41 nm. This finding suggests the development of a nano-device with co-existence of oscillation and rotation.
- (3) When L2 is slightly greater than L1, the two rotors rotate synchronously when driven by a high-speed motor.
- (4) Rotor 2 has no oscillation if L2 is close to the sum of Lm and L1 or if there is a small axial gap between the right or left ends of rotor 1 (together with the motor) and the stator.
- (5) When L2 is no less than 4.91 nm and the rotors are driven by a high-speed (e.g., 200 GHz) motor, it is possible to adjust the synchronous rotation mode of rotor 1 (with either the motor at a lower temperature or with rotor 2 at a higher temperature) by changing the environmental temperature.
- (6) Using different zigzag tube to act as rotor 2, the radii difference between two rotors leads to different output of the rotational frequency and oscillation of the two rotors. At higher temperature, the same rotor 2 has different output rotational speed.

Acknowledgements

The authors are grateful for the financial support from the National Natural-Science-Foundation of China (Grant Nos. 50908190, 11372100).

References

- 1. J. Cumings and A. Zettl, Science, 2000, **289**, 602-604.
- 2. R. Zhang, Z. Ning, Y. Zhang, Q. Zheng, Q. Chen, H. Xie, Q. Zhang, W. Qian and F. Wei, *Nature nanotechnology*, 2013, **8**, 912-916.
- 3. Z. Qin, Q. H. Qin and X. Q. Feng, *Physics Letters A*, 2008, **372**, 6661-6666.
- 4. Q. Zheng and Q. Jiang, *Physical review letters*, 2002, **88**, 045503.
- 5. K. Cai, H. Yin, Q. H. Qin and Y. Li, *Nano letters*, 2014, **14**, 2558-2562.
- 6. A. Subramanian, L. Dong, B. J. Nelson and A. Ferreira, Applied Physics Letters, 2010, 96, 073116.
- 7. W. Qiu, Y. Kang, Z. Lei, Q. H. Qin and Q. Li, Chinese Physics Letters, 2009, 26, 080701.
- 8. W. Qiu, Y. L. Kang, Z. K. Lei, Q. H. Qin, Q. Li and Q. Wang, Journal of Raman Spectroscopy, 2010, 41, 1216-1220.
- 9. S. Zhang, W. K. Liu and R. S. Ruoff, *Nano letters*, 2004, **4**, 293-297.
- 10. C. Zhu, W. Guo and T. Yu, Nanotechnology, 2008, 19, 465703.

- 11. S. Joseph and N. Aluru, *Physical review letters*, 2008, **101**, 064502.
- 12. A. Lohrasebi and Y. Jamali, Journal of Molecular Graphics and Modelling, 2011, 29, 1025-1029.
- 13. J. Zhao, L. Liu, P. J. Culligan and X. Chen, *Physical Review E*, 2009, **80**, 061206.
- 14. K. Cai, H. Cai, H. Yin and Q. H. Qin, RSC Advances, 2015, **5**, 29908-29913.
- 15. K. Cai, H. Cai, J. Shi and Q. H. Qin, *Applied Physics Letters*, 2015, **106**, 241907.
- 16. J. W. Kang and H. J. Hwang, *Nanotechnology*, 2004, **15**, 1633-1638.
- 17. Z. Tu and X. Hu, *Physical Review B*, 2005, **72**, 033404.
- 18. J. Vacek and J. Michl, *Advanced Functional Materials*, 2007, **17**, 730-739.
- 19. Z. Xu, Q.-S. Zheng and G. Chen, *Physical Review B*, 2007, **75**, 195445.
- 20. B. Wang, L. Vuković and P. Král, *Physical review letters*, 2008, **101**, 186808.
- 21. K. Cai, Y. Li, Q. Qin and H. Yin, *Nanotechnology*, 2014, **25**, 505701.
- 22. K. Cai, Y. Li, H. Yin and Q. H. Qin, Mechanics & Industry, 2015, 16, 110.
- 23. A. Fennimore, T. Yuzvinsky, W.-Q. Han, M. Fuhrer, J. Cumings and A. Zettl, Nature, 2003, 424, 408-410.
- 24. R. Saito, R. Matsuo, T. Kimura, G. Dresselhaus and M. Dresselhaus, *Chemical Physics Letters*, 2001, **348**, 187-193.
- 25. A. Barreiro, R. Rurali, E. R. Hernandez, J. Moser, T. Pichler, L. Forro and A. Bachtold, Science, 2008, 320, 775-778.
- 26. M. Hamdi, A. Subramanian, L. Dong, A. Ferreira and B. J. Nelson, *Mechatronics, IEEE/ASME Transactions on*, 2013, **18**. 130-137.
- 27. T. Yuzvinsky, A. Fennimore, A. Kis and A. Zettl, Nanotechnology, 2006, 17, 434-438.
- 28. G. Shan, Y. Wang and W. Huang, *Physica E: Low-dimensional Systems and Nanostructures*, 2011, **43**, 1655-1658.
- 29. K. Kim, X. B. Xu, J. H. Guo and D. L. Fan, Nature communications, 2014, 5, 3632.
- 30. S. J. Stuart, A. B. Tutein and J. A. Harrison, The Journal of chemical physics, 2000, 112, 6472-6486.
- 31. LAMMPS, LAMMPS Molecular Dynamics Simulator. (http://lammps.sandia.gov/), 2013.